Journal of Hydroscience and Hydraulic Engineering
Vol. 19, No.1 May, 2001, 65-74

DIRECT NUMERICAL SIMULATION OF OPEN-CHANNEL TURBULENT FLOW USING A REGULAR GRID IN A GENERALIZED COORDINATE SYSTEM

By

Shunichiro Hayashi

Department of Civil Engineering, Kumamoto Prefectural Government,
6-18-1 Suizenji, Kumamoto, Japan

Terunori Ohmoto

Associate Professor, Department of Civil and Environmental Engineering,
Kumamoto University, 2-39-1 Kurokami, Kumamoto, Japan

and

Ryuichi Hirakawa

Department of Civil and Environmental Engineering,
Kumamoto University, 2-39-1 Kurokami, Kumamoto, Japan

SYNOPSIS

A direct numerical simulation method using a regular grid under a generalized curvilinear coordinate system is presented which can reproduce flows in complex geometries. In this paper, at first a one-dimensional linear convection problem was considered to investigate the accuracy. The results showed that defining a grid with certain types of unequal spacings causes substantial phase errors in numerical solutions due to metric discontinuity. Next, a regular grid under a generalized coordinate system was used to analyze free surface turbulent flow with a Reynolds number of 150 defined by friction velocity. It was shown that this method resulted in sufficiently stable calculations. In addition, a comparison with direct numerical simulation of open channel flow using a staggered grid verified that this simulation gave reasonably satisfactory predicts with respect to high order moments of velocity fluctuations.

INTRODUCTION

Recent advancement in computer technology has offered new insight into the phenomenon of turbulent flows. In particular, the numerical analysis method called direct numerical simulation (DNS), which is purely based on physical laws without a turbulence model, is expected to be very useful because of the versatility and reliability of the Navier-Stokes equations (19). However, application of DNS to turbulent flows with complicated boundary shapes or high Reynolds numbers poses a challenge to engineers who are making various efforts to overcome the related difficulties. While staggered grids have conventionally been used for computation, non-staggered grids are becoming more frequently used. For instance, studies on collocated grid systems have advanced rapidly due to their applicability to generalized coordinate systems (8),(12).

Application of DNS to turbulent channel flow with free surfaces such as rivers and seas was first attempted by Lam

& Banerjee (11). Since then, this approach has provided important information on turbulence structures and mass transport mechanism near free surfaces (Komori, et al (9); Hundler et al (4); Nagaosa and Saito (13),(14); Nezu and Yamamoto (17)), which are difficult to investigate experimentally. All of these studies have employed either the spectral or finite difference method using a staggered grid and there have been no attempts to use a regular grid for calculations.

With the aim of applying DNS to complex boundary flow fields, the authors (3) developed a DNS scheme with good computational accuracy and numerical stability; this was done by using a regular grid in a generalized coordinate system to allow the application to arbitrary boundary conditions and the reduction of computing loads, and also by coupling a high-order accuracy upwind finite difference scheme with a high-order temporal discretization method. As a first step, the DNS scheme was applied to parallel plate flows to make a comparison with a spectral method. A reasonable good agreement was demonstrated by turbulence statistics and the budget of Reynolds stress even on a coarse grid. Thus, the precision and usefulness of the DNS scheme were verified.

In this study, a one-dimensional convection problem is considered to show that setting an unequally spaced grid (non-uniformly spaced grid), together with other aspects, is important to ensure solution accuracy in a regular grid application with a generalized coordinate system. Another aim of this study is to extend the application of DNS using a regular grid in a generalized coordinate system to open channel turbulence for verification of accuracy and effectiveness. Also, properties of free surface flows are discussed in comparison with parallel plate flows.

SETTING OF NON-UNIFORMLY SPACED GRID

Outline of Grid System

Computational grids can be classified into regular and staggered grid systems according to the arrangement of evaluation points of velocity and pressure. Staggered grids have mostly been used in spatial discretization methods of flow analysis either in the MAC or SIMPLE method because staggered grids can suppress numerical vibrations. However, staggered grids require a lot of interpolating operations, and computing loads become tremendous when a generalized coordinate system is used. The selection of a grid system therefore is closely related to the compactness of turbulent flow calculations. By contrast, regular grids are known to suffer from spatial vibrations in the solution (18). However, they are convenient for programming because all physical quantities are defined at the same point. Other benefits of regular grids are suitability for improving the accuracy of the solution and easy conversion into a generalized coordinate system which is effective in dealing with complex boundary problems. Numerical vibrations can be removed by adopting a non-uniformly spaced grid (3) so that efficient simulation can be realized by using a coarse grid over the areas where spatial changes of velocity are small, except a near-wall region.

Effect of Non-Uniformly Spaced Grid

Since adoption of the non-uniformly spaced grid generally decreases accuracy, the effects of this type grid on the numerical solution are discussed here for a one-dimensional linear convection problem (7) given by Eq.1.

$$\frac{\partial u}{\partial t} + U\frac{\partial u}{\partial x} = 0, \qquad (U = 1,\ -\infty < x < \infty)$$

$$u(x,0) = \begin{cases} \dfrac{1-\cos(2x-\pi)}{2}, & (\dfrac{\pi}{2} \le x \le \dfrac{3\pi}{2}) \\ 0, & otherwise \end{cases} \qquad (1)$$

As shown in Figure 1, three types of grids are used: a uniformly spaced grid, a smooth non-uniformly spaced grid (A) with continuous metric x_ξ, and a smooth non-uniformly spaced grid (B) with discontinuities in metric x_ξ. Since the

exact solution of Eq.1 is actually identical to the initial waveform and does not change with time, the numerical solution after the m-th cycle is compared with the exact solution by adopting periodic boundary conditions in the x-direction. The third-order Adams-Bashforth scheme is used for temporal integration (3).

Figure 2 presents a comparison of waveforms after 50 cycles of computation for a Courant number of 0.1. Graphs (a) through (c) in the upper part are based on a central difference scheme, whereas graphs (d) through (f) in the lower part are based on an upwind difference scheme.

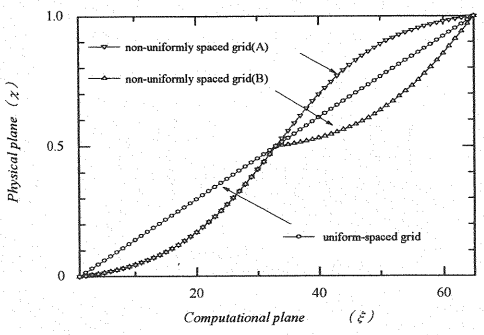

Fig. 1 Coordinate transformation

The non-uniformly spaced grid (A) results in a slightly greater attenuation error than the uniformly spaced grid. This is probably caused by the fact that accuracy is diminished by one order when the grid spacing does not change smoothly in a non-uniformly spaced grid, as can be inferred from the truncation error of the second-order differential approximation deduced by the Taylor expansion (2),(6). Graphs (c) and (f) suggest that this accuracy loss can be compensated by adopting a higher-order finite difference approximation. As for the non-uniformly spaced grid (B), not only attenuation error but also phase error are generated in all cases. Because this grid has the same smoothness as the non-uniformly spaced grid (A), the phase error would appear to be related to discontinuities in the metric x_{ξ}.

Regarding the finite difference scheme of convection terms, upwind difference schemes can be expressed as a sum of central differences and the numerical viscosity term. Therefore, the central difference schemes of graphs (a) through (c) become the upwind difference schemes of graphs (d) through (f) by adding the second-, fourth-, and sixth-order differential truncation errors (numerical viscosity), respectively. Accordingly, the effect of numerical viscosity can be investigated by comparing the graphs in the upper part of Figure 2 with those in the lower part. While numerical viscosity has the effect of suppressing vibrating solutions found in the central difference, the effect is more profound in lower-order upwind differences so that the solution itself becomes skewed. Even third-order upwind differences, which are often used in practical computations, are not suited for turbulence calculations in which very high accuracy is required. The fifth-order upwind difference functions as a high-cut filter that removes only high-wavenumber components with little adverse effect on solutions. In central differences, even in the case of high order accuracy, nonlinear instability is likely to be triggered by dispersibility caused by odd-numbered differential truncation errors (5). By contrast, the fifth-order upwind difference is effective in removing aliasing errors caused by high-wave number components continuously generated from nonlinear terms and in suppressing numerical vibrations having no physical meaning. Accordingly, in the present study's analysis using a regular grid in a generalized coordinate system, a non-uniformly spaced grid with sufficient smoothness and a continuous metric is generated, and the fifth-order upwind difference scheme is used for the convection term.

NUMERICAL SIMULATION OF OPEN CHANNEL FLOW

Flow Configuration

We simulated a fully developed turbulent flow in an open channel with a solid bottom and a free surface, applying the zero Froude number approximation (1) that permits no deformation, as shown in Figure 3. Periodic boundary conditions are given to the streamwise and spanwise directions, so that the flow field is free from the effect of side walls. The flow is induced by gravity, and correspondingly the x-axis makes an angle θ with the horizontal. The relationship between friction velocity and gravity is given by

$$u_\tau = \sqrt{gh\sin\theta} \qquad (2)$$

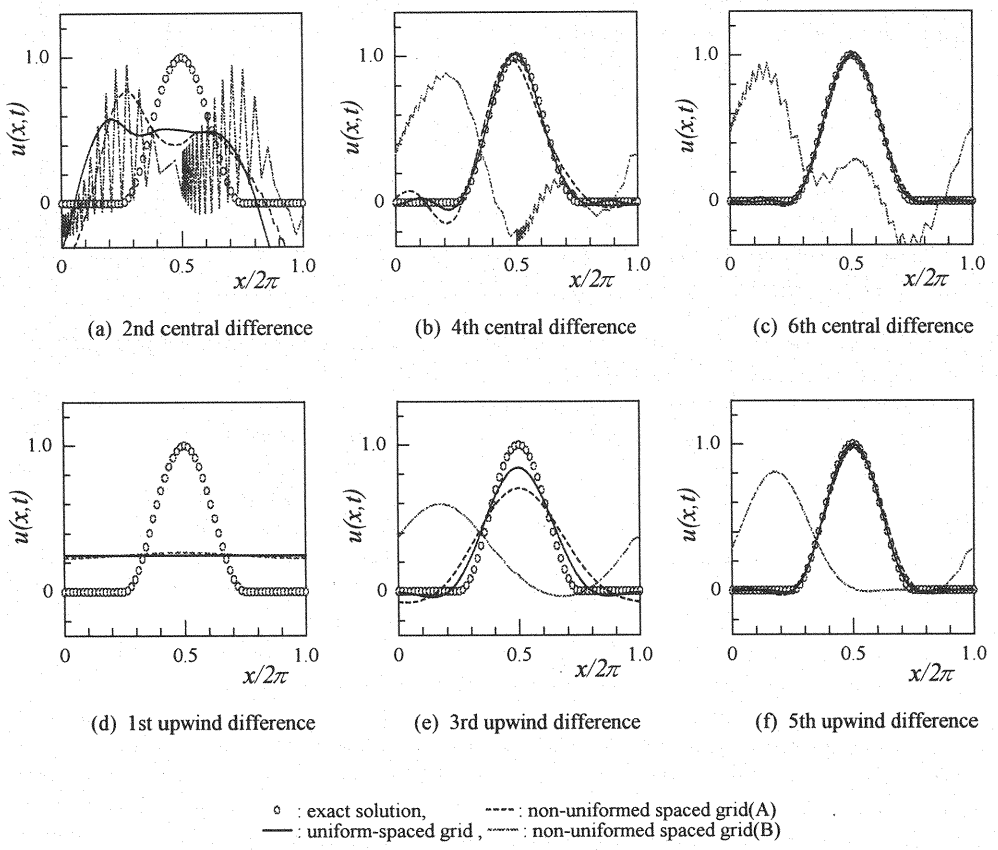

Fig. 2 Comparison of waveforms for different types of grid spacing (c = 0.1, $x/2\pi$ = 50)

When reference pressure is defined by equilibrium between gravity and static pressure, and the relationship between friction velocity and average pressure gradient is used, non-dimensional gravity is equivalent to setting the average pressure gradient to -1. Therefore, the effect of gravity can be incorporated into the computation by including the average pressure gradient in the x-direction. As a result, Reynolds number becomes the only variable parameter in the present computation. To make a comparison with the results of Nagaosa (19) obtained with a staggered grid, the computational domain was set to have a water depth h, streamwise length $2\pi h$ and spanwise width πh in the case of a Reynolds number of 2280 defined by the mean velocity and depth. This figure corresponds to a Reynolds number defined by friction velocity of about 150, and the computational domain can be indicated by inner variables as $x^+ \fallingdotseq 942$, $y^+ \fallingdotseq 150$, and $z^+ \fallingdotseq 471$. A fine grid of $96 \times 97 \times 96$ and a coarse grid of $64 \times 65 \times 64$ were used to investigate the effect of grid spacing on upwind finite differences. Taking the discussion on grid generation in the previous chapter into account, a hyperbolic tangent (tanh) that is smooth with a continuous metric x_ξ was used. Figure 4 shows a longitudinal section of the coarse grid, where the simulation was efficiently intended in accordance with flow properties; a sufficient number of grid points were arranged to enhance the spatial resolution in the free surface region and the wall region (spanning from the viscous sublayer to the buffer layer) where the wall turbulence is active. Grid points were less densely arranged in the intermediate region. As a result, spatial resolution was about $\Delta x^+ = 9.8$, $\Delta y^+ = 0.1$-2.8, and

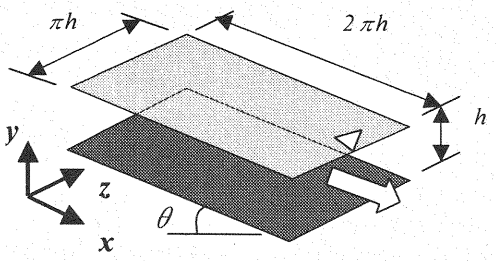

Fig. 3 Flow geometry and axes system

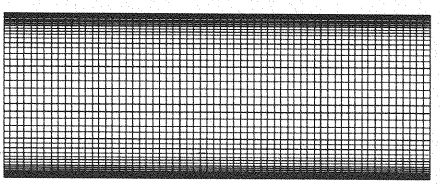

Fig. 4 Coarse grid generation (x-y section)

$\Delta z^+ = 4.9$ in the fine grid, and $\Delta x^+ = 14.7$, $\Delta y^+ = 0.1$-6.7, and $\Delta z^+ = 7.4$ in the coarse grid.

Computational Method

The continuity and Navier-Stokes equations were the basic formulas to be solved, and the MAC method was adopted for the solution of pressure. Because the flow field is an open channel between a flat bottom and a free-slip top surface, coordinate axes are perpendicular to each other. Therefore, the variable conversion is a one-dimensional coordinate transformation given by

$$x = x(\xi), \quad y = y(\eta), \quad z = z(\zeta) \tag{3}$$

Applying the chain rule to the above equation, and expressing the first- and second-order differential in the computational plane, the Navier-Stokes equation becomes

$$\begin{aligned}
&\frac{\partial u}{\partial t} + \frac{u}{x_\xi}\frac{\partial u}{\partial \xi} + \frac{v}{y_\eta}\frac{\partial u}{\partial \eta} + \frac{w}{z_\zeta}\frac{\partial u}{\partial \zeta} = -\frac{1}{x_\xi}\frac{\partial p}{\partial \xi} \\
&\quad + \frac{1}{\mathrm{Re}}\left(\frac{1}{x_\xi^2}\frac{\partial^2 u}{\partial \xi^2} - \frac{x_{\xi\xi}}{x_\xi^3}\frac{\partial u}{\partial \xi} + \frac{1}{y_\eta^2}\frac{\partial^2 u}{\partial \eta^2} - \frac{y_{\eta\eta}}{y_\eta^3}\frac{\partial u}{\partial \eta} + \frac{1}{z_\zeta^2}\frac{\partial^2 u}{\partial \zeta^2} - \frac{z_{\zeta\zeta}}{z_\zeta^3}\frac{\partial u}{\partial \zeta} \right) \\
&\frac{\partial v}{\partial t} + \frac{u}{x_\xi}\frac{\partial v}{\partial \xi} + \frac{v}{y_\eta}\frac{\partial v}{\partial \eta} + \frac{w}{z_\zeta}\frac{\partial v}{\partial \zeta} = -\frac{1}{y_\eta}\frac{\partial p}{\partial \eta} \\
&\quad + \frac{1}{\mathrm{Re}}\left(\frac{1}{x_\xi^2}\frac{\partial^2 v}{\partial \xi^2} - \frac{x_{\xi\xi}}{x_\xi^3}\frac{\partial v}{\partial \xi} + \frac{1}{y_\eta^2}\frac{\partial^2 v}{\partial \eta^2} - \frac{y_{\eta\eta}}{y_\eta^3}\frac{\partial v}{\partial \eta} + \frac{1}{z_\zeta^2}\frac{\partial^2 v}{\partial \zeta^2} - \frac{z_{\zeta\zeta}}{z_\zeta^3}\frac{\partial v}{\partial \zeta} \right) \\
&\frac{\partial w}{\partial t} + \frac{u}{x_\xi}\frac{\partial w}{\partial \xi} + \frac{v}{y_\eta}\frac{\partial w}{\partial \eta} + \frac{w}{z_\zeta}\frac{\partial w}{\partial \zeta} = -\frac{1}{z_\zeta}\frac{\partial p}{\partial \zeta} \\
&\quad + \frac{1}{\mathrm{Re}}\left(\frac{1}{x_\xi^2}\frac{\partial^2 w}{\partial \xi^2} - \frac{x_{\xi\xi}}{x_\xi^3}\frac{\partial w}{\partial \xi} + \frac{1}{y_\eta^2}\frac{\partial^2 w}{\partial \eta^2} - \frac{y_{\eta\eta}}{y_\eta^3}\frac{\partial w}{\partial \eta} + \frac{1}{z_\zeta^2}\frac{\partial^2 w}{\partial \zeta^2} - \frac{z_{\zeta\zeta}}{z_\zeta^3}\frac{\partial w}{\partial \zeta} \right)
\end{aligned} \tag{4}$$

Likewise, the Poisson equation for pressure corresponding to the continuity equation is expressed in the computational plane by

$$\frac{1}{x_\xi^2}\frac{\partial^2 p}{\partial \xi^2}-\frac{x_{\xi\xi}}{x_\xi^3}\frac{\partial p}{\partial \xi}+\frac{1}{y_\eta^2}\frac{\partial^2 p}{\partial \eta^2}-\frac{y_{\eta\eta}}{y_\eta^3}\frac{\partial p}{\partial \eta}+\frac{1}{z_\zeta^2}\frac{\partial^2 p}{\partial \zeta^2}-\frac{z_{\zeta\zeta}}{z_\zeta^3}\frac{\partial p}{\partial \zeta}=$$

$$\left(\frac{1}{x_\xi}\frac{\partial u}{\partial \xi}+\frac{1}{y_\eta}\frac{\partial v}{\partial \eta}+\frac{1}{z_\zeta}\frac{\partial w}{\partial \zeta}\right)\Big/\Delta t \tag{5}$$

Using the above basic equations, the analysis was conducted by a fractional step algorithm shown below. In an evolution equation to deduce an intermediate velocity field, the explicit third-order Adams-Bashforth method was used for the nonlinear term, and the implicit second-order Crank-Nicolson method was used for the viscous term. These features simultaneously allow removal of temporal phase errors (3), compactness by the explicit solution method, good convergence and numerical stability by the implicit solution method, and reduction of the overall volume of the solution by separating velocity and pressure as expressed by,

$$\frac{\tilde{U}-U^n}{\Delta t}=\frac{1}{12}\left(23H^n-16H^{n-1}+5H^{n-2}\right)+\frac{1}{2\mathrm{Re}}\nabla^2\left(\tilde{U}+U^n\right) \tag{6}$$

$$\nabla^2 p^{n+1}=\frac{div\,\tilde{U}}{\Delta t} \tag{7}$$

$$\frac{U^{n+1}-\tilde{U}}{\Delta t}=-grad\ p^{n+1} \tag{8}$$

where, H represents the convection term and n expresses the time level. Fourth-order discretization of the Poisson equation for pressure was performed, and the velocity field of a new step was calculated by applying the Euler's backward scheme to pressure. The plane Gauss-Seidel method was used for an iterative solution of (6) and (7). The non-slip boundary condition was applied to the bottom surface. On the free surface, the slip condition was applied to velocity components u, w and v was set to zero.

RESULTS AND DISCUSSION

Since a DNS database on free surface turbulent flows has not been established, the accuracy in the present study was verified by making comparisons with the results obtained by Nagaosa (15) and a representative database of parallel

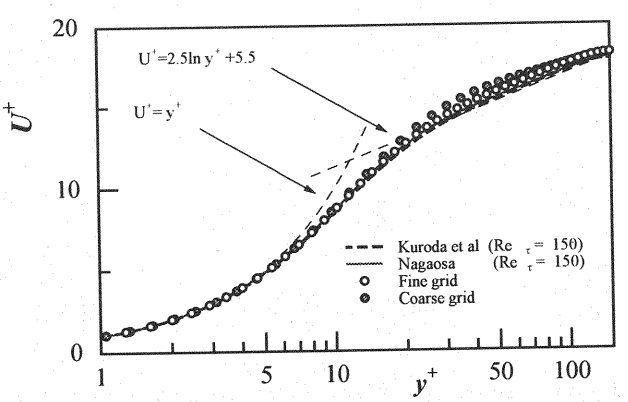

Fig.5 Mean velocity distribution

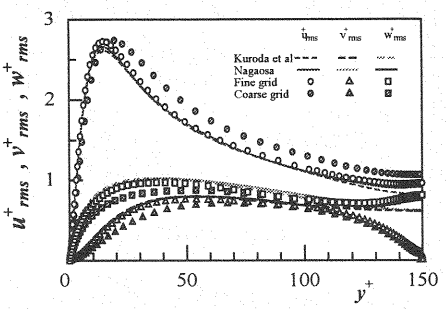

Fig.6 Turbulence intensity

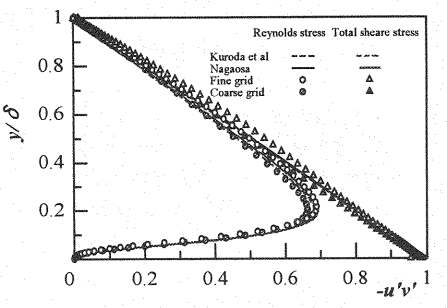

Fig.7 Reynolds stress and Total shear stress

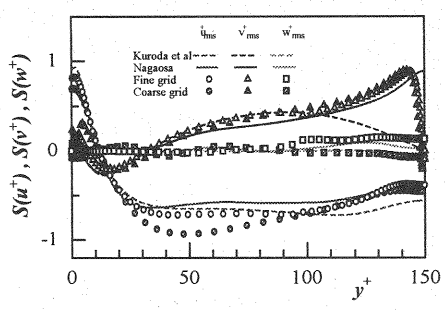

Fig.8 Skewness factor

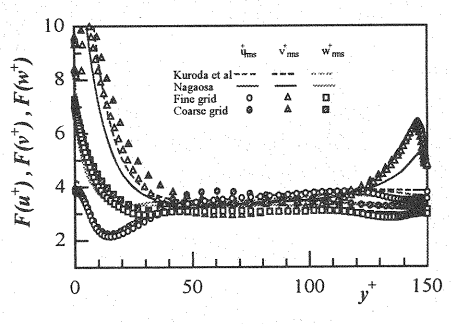

Fig.9 Flatness factor

plate flows (10) obtained by Kuroda et al. Turbulence statistics were calculated from a time average of 100,000 steps ($\Delta t = 2/1000*h/u_\tau$).

Figure 5 shows mean velocity distributions. The results of our computation are generally in good agreement with Nagaosa's data, and little difference was found between the fine and coarse grids when turbulence was fully developed. However, the coarse grid resulted in slightly greater velocity than the fine grid in the logarithmic law region. When spatial resolution was low, the mean velocity distribution became similar to the distribution of laminar flow as with low-order upwind differences with significant numerical viscosity (3). While a 'velocity-dip' phenomenon of the maximum velocity below the free surface is often observed in open channel flows, this phenomenon was not observed in this study. This is probably because side wall effects were eliminated by assuming the span to be infinite.

Figure 6 shows turbulence intensity distributions. The results of the fine and coarse grids, in comparison with Nagaosa's data, are somewhat different; u^+_{rms} was overestimated while v^+_{rms} and w^+_{rms} were underestimated on the coarse grid. Compared with the case of a closed channel, disturbances near the free surface were restricted in the depth direction and enhanced in the mean stream and span directions; this enhanced anisotropy of turbulence by redistribution is a characteristic of free surface turbulence. In comparison with parallel plate flows, a significant difference between closed channel and open channel flows was observed only in the free surface region corresponding to the outer layer (16) ($0.6 < \xi < 1.0$). However, no difference was observed between parallel plate and open channel flows in the near-wall region, where the effect of the free surface is negligible.

Figure 7 shows distributions of Reynolds stress and total shear stress. The results of the fine and coarse grids are in good agreement with the Nagaosa's data, and there is not much difference between the two types of grids when turbulence is fully developed. There is no difference in Reynolds stress or total shear stress between closed channel flow and open channel flow.

Figures 8 and 9 show skewness and flatness factors, which correspond to the third- and fourth-order moments of

velocity fluctuations, respectively. While our results generally agree with Nagaosa's results, the skewness and flatness of the fluctuation of v exhibit different trends near the free surface. While the skewness of the fluctuation of v increases monotonously toward the free surface in Nagaosa's data, our data show a marked decrease beyond $y^+ = 140$. Our data also show a prominent peak in the flatness of the fluctuation of v near $y^+ = 140$. It should be noted, however, that our data could not be directly compared with Nagaosa's data, which were obtained by coupling scalar transport equations. Additional accurate experimental measurements of turbulence statistics near the free surface are required.

Closed channel flows are similar to open channel flows in which the distributions of mean velocity and Reynolds stress are little affected by the free surface, and any difference in turbulence intensity is restricted to the free surface region. On the other hand, difference in skewness is prominent even in the intermediate region. This may be related to boils that are not observed in closed channel flow, and more detailed investigations are required in this regard. Because free surface fluctuations and the Froude number were small for the Reynolds number used in this study (1), and the effect of the free surface was restricted, as discussed above, to the area near the surface, the zero Froude approximation without taking deformation into account as a boundary condition is considered to be a reasonable approach.

CONCLUSIONS

We first investigated the effect of a non-uniformly spaced grid on the accuracy of solution by dealing with a one-dimensional linear convection problem. DNS of open channel turbulent flow was then conducted using a regular grid in a generalized coordinate system to compare mean flow characteristics and turbulence statistics with existing data. The following conclusions were obtained from the results :

1) When mapping is conducted by coordinate transformation, large phase errors may occur when there are discontinuities in metric x_ξ. With generation of a non-uniformly spaced grid, therefore, smoothness and metric continuity should be ensured to avoid loss of accuracy caused by spatial discretization.
2) Even if grid points for computing are based on a regular grid in a generalized coordinate system, computation can be perfectly conducted without instability or spatial vibration by using an appropriate non-uniformly spaced grid.
3) Numerical results with high accuracy were obtained from a test computation for an open channel turbulent flow, although some dependence on grid spacing was observed. Considering the ease of handling and reduction in computing loads, a regular grid can be very useful for spatial discretization.

The computational method developed in this study can be executed with a commercial personal computer and is considered to be very useful for engineering purposes. The computing time per step on a coarse grid was about 7 sec using Visual Technology's VT-Alpha 600 .

ACKNOWLEDGEMENT

We are grateful to Dr. R. Nagaosa of the Agency of Industrial Science and Technology's National Institute for Resources and Environment for generously supplying the DNS data of free surface flows used for comparison in this study.

REFERENCES

1. Daiguji,H.,Miyake,Y.,Yoshizawa,A. ed. : Computational Fluid Dynamics of Turbulent Flow - Models and Numerical Methods, Univ.Tokyo press,1998. (in Japanese)
2. Fujii,K. : Numerical Methods for Computational Fluid Dynamics, Univ.Tokyo press, 1994. (in Japanese)
3. Hayashi,S.,Ohmoto,T.,Yakita,K.,Hirakawa,R. : Fundamental study on direct numerical simulation using upwind difference scheme, J.Applied Mechanics, JSCE, Vol.2, pp.599-608, 1999. (in Japanese)
4. Handler,R.A.,Swean,T.F.,Jr.,Leighton,R.I.,and Swearingen,J.D. : Length scale and the energy balance for turbulence near a

free surface, AIAA J.,31, pp.1998-2007, 1993.

5. JSCE : Introduction to Numerical Simulation for Wind Engieering, 1992.
6. JSME : Fundamentals of Computational Fluid Dynamics, Corona pub., 1988. (in Japanese)
7. Kajishima,T. : Upstream-shifted interpolation method for numerical simulation of incompressible flows, JSME, Vol.60-578B, pp.3319-3326, 1994. (in Japanese)
8. Kajishima,T.,Ohta,T.,Okazaki,K.,Miyake,Y. : High-order finite-difference method for incompressible flows using collocated grid system, JSME, Vol.63-614B, pp.3247-3254, 1997. (in Japanese)
9. Komori,S.,Nagaosa,R.Murakami,Y.,Chiba,S.,Ishii,K.and Kuwahara,K:Direct numerical simulation of three-dimensional open-channel flow with zero-shear gas-liquid interface, Phys.Fluids A,5, pp.115-125, 1993.
10. Kuroda,A.,Kasagi,N. : Establishment of the direct numerical simulation data base of turbulent transport phenomena, Co-operative Research, Ministry of education science and culture, 1992. (in Japanese)
11. Lam,K.and Banerjee,S. : On the condition of streak formation in a bounded turbulent flow, Phys.Fluids A, 4, pp.306-320, 1992.
12. Morinishi,Y. : An improvement of collocated finite difference scheme with regard to kinetic energy conservation, JSME, Vol.65-630B, pp.505-512, 1999. (in Japanese)
13. Nagaosa,R.,Saito,T. : Turbulence structure in stably stratified open-channel flows, JSME, Vol.63-608B, pp.1170-1176, 1997. (in Japanese)
14. Nagaosa,R.,Saito,T. : On the relationship between the coherent structure and heat and mass transfer mechanism near a free surface in a fully developed turbulence, JSME, Vol.64-620B, pp.1025-1032, 1998. (in Japanese)
15. Nagaosa,R. : Direct numerical simulation of vortex structures and turbulent scalar transfer across a free surface in a fully developed turbulence, Phys.Fluids,Vol.11,No.6,pp1581-1595, 1999.
16. Nezu,I. ,Nakagawa,H. : Turbulence in Open-Channel Flows, IAHR-Monograph,Balkema, 1993.
17. Nezu,I.,Yamamoto,Y. : Analysis of the processes of production and transportation of turbulence in cavity open-channel flows by DNS, J.Hydraulic Eng., JSCE, Vol.43, pp.377-382. 1999. (in Japanese)
18. Patankar,S.V. : Numerical Heat Transfer and Fluid Flow, Hemisphere, 1985.
19. Tatsumi,T. : Navier-Stokes equation and turbulence, The 44th Nat.cong.of theoretical & applied machanics, pp.7-11, 1995. (in Japanese)

APPENDIX – NOTATION

The following symbols are used in this paper :

F	= flatness factor ;
H	= convection term ;
p	= pressure ;
Re	= Reynolds number ;
S	= skewness factor ;
t	= time ;
u_τ	= friction velocity ;
u,v,w	= instantaneous velocities in the x , y and z direction ;
$-u'v'$	= Reynolds stress

U,V,W = mean velocities in the x, y and z direction ;

$\tilde{U}$ = intermediate velocity ;

x,y,z = coordinates in the physical plane ;

x,y,z = coordinates of streamwise,vertical and spanwise direction ;

Δt = time increment ;

Δx, Δy, Δz = spatial increment in the x, y and z direction ;

Δx^+, Δy^+, Δz^+ = dimensionless spatial increment in the coordinate x, y and z direction ;

δ = channel half-width ;

η_j = coordinates in the computational plane ; and

ν = kinematic viscosity of fluid.

The superscript

$+$ = non-dimensional coordinate normalized by the viscous length.

The subscript

$r.m.s$ = root mean square value.

(Received August 28, 2000 ; revised November 29, 2000)